Controllable Organization of Quantum Dots into Mesoscale Wires and Cables via Interfacial Block Copolymer Self-Assembly

Robert B. Cheyne and Matthew G. Moffitt*

Department of Chemistry, University of Victoria, P.O. Box 3065, Victoria, BC V8W 3V6, Canada

Received October 12, 2006; Revised Manuscript Received January 23, 2007

ABSTRACT: This paper describes morphology control and characterization of interfacial properties for the synergistic self-assembly of polymer-stabilized CdS quantum dots (QDs), referred to as PS-CdS, with polystyrene-*block*-poly(ethylene oxide) (PS-*b*-PEO) diblock copolymers at the air−water interface. This spontaneous process yields various hierarchical one-dimensional (1D) QD/polymer hybrid structures with widths commensurate with optical wavelengths, ∼300 nm, including wires, cables, branched wires, and rings incorporated along the lengths of cables. Control over predominant hybrid assemblies is achieved by varying the PS-CdS/PS-*b*-PEO blend composition and the concentration of the spreading solution, with higher PS-CdS fractions resulting in more uniform distributions of QDs throughout hybrid structures and higher spreading concentrations giving rise to a greater predominance of 1D structures relative to circular dots and island aggregates. Compression isotherms of QD/polymer assemblies at the air−water interface reveal that interfacial behavior of aggregates is also dependent on the spreading conditions and blend composition; for all spreading concentrations, a maximum is observed in plots of the limiting area vs PS-CdS weight fraction in the blends, suggesting a competition between the conformational effects of PS-*b*-PEO dilution and PS-CdS addition. In addition, we describe a mechanism of formation for QD/polymer assemblies, based on AFM data of structures obtained at the highest spreading concentration, in which self-assembly is initiated by dewetting of the evaporating polymer solution from the air−water interface.

Introduction

Colloidal metal and semiconductor nanoparticles have been recognized as promising building blocks for a new generation of photonic and electronic devices due, in part, to their unique and size-dependent properties arising from quantum confinement and surface effects.[1] Essential to the production of devices and materials with specific function will be the organization of nanoparticles on solid substrates into ordered patterns with well-defined length scales. To this end, a variety of research efforts have coupled self-assembly processes to the patterning of nanoparticle building blocks into hierarchical one- and two-dimensional superstructures with organization on multiple length scales.[2−21]

Various equilibrium and nonequilibrium self-assembly processes have been successful in patterning of nanoparticles on surfaces. Passivated nanocrystals have been patterned into 2D circles and extended stripes via interparticle interactions at the air−water interface under equilibrium conditions[5] as well as through nonequilibrium, drying mediated processes on surfaces.[9,11,13] Self-assembly strategies that combine control of nanoparticle organization with incorporation into a polymeric matrix offer additional possibilities for tuning the mechanical, optical, electronic, magnetic, and catalytic properties of new nanostructured composites.[3,4,13−21] Along with the many attractive physical properties of the polymer component in such hybrid materials, self-assembling polymer systems offer unique possibilities for mediating the assembly of nanoparticles into a wide range of structures exhibiting organization on various length scales.[14] We[21] and others[19,20] have recently employed polymer/polymer phase separation as a strategy for obtaining micron-scale patterns of nanoparticles on surfaces. Block copolymers have also been widely used to organize nanoparticles by promoting their localization within specific domains arising from microphase separation.[14−18] The vast majority of these studies have employed block copolymers in the solid state, where domain patterns are highly ordered and feature sizes are limited by the dimensions of a polymer chain, on the order of tens of nanometers.

In a recent letter, we described a very different approach to the use of block copolymers for the organization of semiconductor nanoparticles, or quantum dots (QDs), in which self-assembly occurs at the air−water interface.[22] The self-assembly of block copolymers at the air−water interface is well-known to result in a wide range of nanoscale surface aggregates.[23,24] For example, in the case of polystyrene-*block*-poly(ethylene oxide) (PS-*b*-PEO) diblock copolymers, interfacial self-assembly is the result of a competition between the aggregation of hydrophobic PS blocks and the spreading of epiphilic (surface-loving) PEO blocks.[25−28] In many cases, the formation of structures arising from this tug-of-war of driving forces is ultimately trapped by vitrification of the PS blocks when the spreading solvent evaporates, resulting in kinetically frozen aggregates that can be transferred to solid substrates using Langmuir−Blodgett (LB) techniques.[25,26] Depending on the relative molecular weights of the blocks and the concentration of the spreading solution, a wide range of surface morphologies can be formed, including dots, spaghetti (wires), planar "continents", rings, and chainlike aggregates.

In order to exploit the self-assembly properties of PS-*b*-PEO diblock copolymers at the air−water interface for the organization of QDs, we first synthesized cadmium sulfide (CdS) QDs inside a polystyrene-*block*-poly(acrylic acid) (PS-*b*-PAA) template, to yield hybrid PS-CdS building blocks (Scheme 1). These colloidal particles consist of a CdS QD core surrounded by two layers of the respective copolymer blocks: an ionically cross-linked, high-T_g poly(cadmium acrylate) layer at the QD surface provides kinetic stability for an outer brush layer of PS chains,

* To whom correspondence should be addressed.

10.1021/ma062355u CCC: $37.00
Published on Web 02/23/2007

Scheme 1. Structure of Block Copolymer-Stabilized Cadmium Sulfide Quantum Dots (PS-CdS)

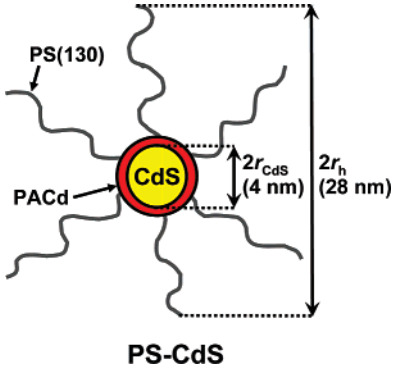

which gives the CdS QDs solubility in various organic solvents and allows dispersion in polymer media. By casting various blend solutions of PS-CdS and PS-*b*-PEO in chloroform at the air−water interface, we have shown that synergistic self-assembly of the two components occurs upon spreading and solvent evaporation.[22] The resulting combination of interactions gives rise to various one-dimensional (1D) QD/polymer surface features, including branched wires, cables, and wires with incorporated rings, which are entirely distinct from superstructures arising from self-assembly of nanoparticles and block copolymers in the bulk. First, the widths of 1D QD/polymer aggregates arising from self-assembly at the air−water interface (∼300 nm) are on the order of optical wavelengths,[22] an order of magnitude larger than domain sizes via block copolymer self-assembly in the bulk.[14] In addition, whereas microphase separation of block copolymers in the bulk state gives rise to highly periodic structures, a wide range of controllable but nonperiodic structures are obtained by the present method, which represent potentially interesting architectures that cannot be achieved in more highly ordered self-assembling systems. This combination of features makes the present strategy for QD organization extremely interesting for bottom-up routes to potential photonic structures, including active waveguides of various geometries for photonic circuits.[29]

In the present paper, we describe the first detailed characterization of structure and dimensions of these QD/polymer surface features as a function of spreading concentration and blend composition. This study shows a number of reproducible trends in the characteristics of 1D QD/polymer aggregates, clearly indicating that self-assembly of the two components can be reliably tuned via the proper choice of spreading conditions. Along with morphological characterization of transferred LB films, we show for the first time that the interfacial behavior of QD/polymer aggregates at the water surface also varies with spreading conditions, by comparing features of Langmuir compression isotherms following evaporation of the spreading solvent. Finally, we propose a mechanism for QD/polymer aggregate formation at the air−water interface based on surface morphologies obtained from the highest spreading concentration, where a greater extent of chain entanglements in the spreading solution results in trapping of earlier stages of self-assembly upon solvent evaporation. Under these conditions, we observe various kinetically frozen transition structures which suggest that dewetting of evaporating blend solutions from the water surface plays a key role in the initial stages of self-assembly.

Experimental Section

Materials. Block copolymer-stabilized CdS QDs (PS-CdS) were prepared via a template approach starting from a polystyrene-*block*-poly(*tert*-butyl acrylate) (PS-*b*-P*t*BA) diblock copolymer, which was synthesized using anionic polymerization techniques; the interested reader is directed to other sources for further information on the synthesis of the copolymer.[30,31] The characteristics of the PS-*b*-P*t*BA polymer are given in Table 1, where M_n is the number-average molecular weight, M_w is the weight-average molecular weight, M_w/M_n is the polydispersity index, and x_n is the number-average degree of polymerization of each given block.

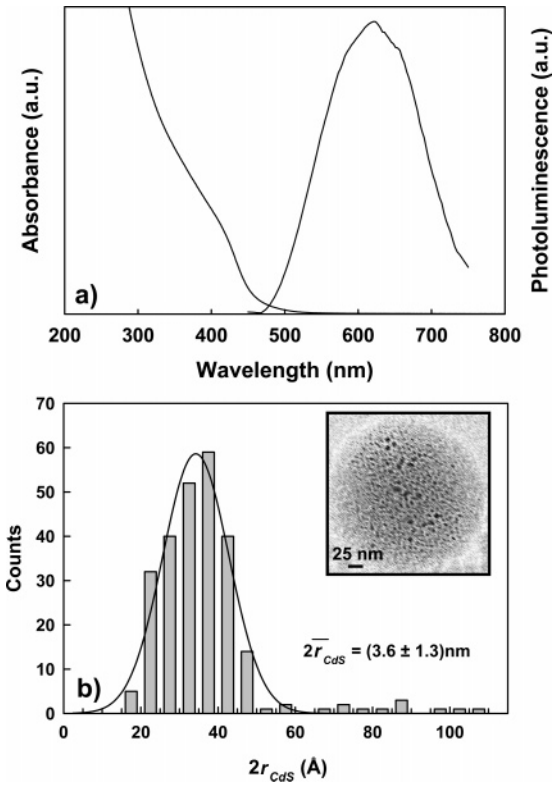

Figure 1. (a) UV−vis absorption and photoluminescence spectra of PS-CdS in chloroform and (b) size distribution of QD diameters observed via transmission electron microscopy (TEM). Inset is a typical TEM image of CdS QDs within an island of PS-CdS after deposition at the air−water interface. Black dots are CdS NPs, and the gray area is PS.

Two different PS-*b*-PEO copolymer samples (Polymer Source) were employed to direct the interfacial self-assembly of PS-CdS, and characteristics of both copolymers are summarized in Table 2. Both copolymers are hydrophobic, with PS blocks that are long relative to the PEO blocks, though the 185K copolymer possesses a somewhat higher PEO content (18.9 wt %) compared to the 141K copolymer (11.4 wt %).

Preparation of Block Copolymer-Stabilized Cadmium Sulfide Quantum Dots (PS-CdS). Starting with the PS-*b*-P*t*BA copolymer described in Table 1, the PS-CdS building blocks were synthesized in a process that involves hydrolysis of PS-*b*-P*t*BA and micellization of PS-*b*-PAA to form block ionomer reverse micelles containing cadmium ions, followed by templated growth of a single CdS QD within each micelle core.[32] Further experimental details are provided in the Supporting Information and in earlier papers from our group.[21,33]

Dynamic Light Scattering (DLS). Dynamic light scattering (DLS) experiments were carried out on a Brookhaven Instruments photon correlation spectrometer equipped with a BI-200SM goniometer, a BI-9000AT digital autocorrelator, and a Melles Griot He−Ne Laser (632.8 nm) with maximum power output of 75 mW. Further details on experimental procedure for DLS measurements and data analysis can be found in the Supporting Information.

UV−Vis Absorption and Photoluminescence Spectroscopy. UV−vis absorption features from the CdS QD core of PS-CdS were used to determine the mean size of the CdS nanoparticles on the basis of the effect of quantum confinement. UV−vis absorption

Table 1. Characteristics of Polystyrene-*block*-poly(*tert*-butyl acrylate) Copolymer Used To Prepare PS-CdS Hybrid Nanoparticles

	M_n (g mol^{-1})	M_w (g mol^{-1})	M_w/M_n	$M_{n,PS}$ (g mol^{-1})	$x_{n,PS}$	$M_{n,PtBA}$ (g mol^{-1})	$x_{n,PtBA}$
PS-*b*-P*t*BA	14 600	15 200	1.04	1500	130	1500	20

spectroscopy of PS-CdS particles dispersed in chloroform were carried out on a Varian Cary 50 UV−vis spectrometer. Static photoluminescence measurements were recorded on an Edinburgh Instruments FLS 920 instrument equipped with a Xe 450 W arc lamp and a red-sensitive PMT (R928-P). The emission spectrum of PS-CdS in chloroform solution was collected at 1 nm spectral resolution using an excitation wavelength of 400 nm.

Surface Pressure−Area Isotherms of PS-CdS/PS-*b*-PEO Langmuir Films. Surface pressure−area (π−A) isotherms and LB thin films were obtained using a KSV 3000 Langmuir trough (KSV Instruments Ltd.) secured inside a dust shield. The total trough surface area was 150 × 515 mm^2, and the total trough volume was ∼1 L. The trough area was robotically controlled by two hydrophobic paddles, which compressed the spread film symmetrically and bilaterally at a rate of 10 mm/min. House-distilled, deionized water (Barnstead NANOpure Diamond, 18.2 mΩ•cm) was used as the subphase in all trials. For all experiments, the subphase temperature was 21 ± 0.5 °C. Prior to each trial, the water surface was cleaned by aspirating off any debris such that the surface pressure remained <0.20 mN/m over a full compression. The LB components were cleaned daily with absolute ethanol before replacing the deionized water subphase. Surface pressure measurements were made from a roughened platinum Wilhemly place (perimeter of 39.240 mm), which was flamed prior to each trial to ensure cleanliness.

PS-CdS spreading solutions were prepared from 4 mg/mL stock solution in spectroscopic grade chloroform (99.9+%, Aldrich). The stock solution was filtered through two 0.45 μm pore diameter Teflon filters (Target) followed by dilution with chloroform to a concentration of 2.0 mg/mL. To prepare PS-CdS spreading solutions of various concentrations, the 2.0 mg/mL solution was then diluted by adding various amounts of filtered chloroform. PS-*b*-PEO solids were dried overnight in a dark desiccator, weighed, and used directly to prepare a 2.0 mg/mL stock solution, also in spectroscopic grade chloroform, from which all other solutions were prepared. For PS-CdS/PS-*b*-PEO blend solutions, five stocks of each component were separately made at concentrations of 2.0, 1.0, 0.50, 0.25, and 0.10 mg/mL. Various blend solutions were then prepared by mixing PS-CdS and PS-*b*-PEO solutions in appropriate ratios into new, cleaned (3 times with acetone, 3 times with spec grade chloroform) vials, to give blends with various PS-CdS weight fractions (f) and total polymer concentrations.

In a typical isotherm experiment, a constant cumulative mass of 0.10 mg solids (PS-CdS + PS-*b*-PEO) was deposited dropwise from an appropriate volume of solution contained in a gastight Hamilton microsyringe onto a clean air−water interface of the Langmuir trough. After an elapsed time of 15 min (to allow for solvent evaporation) the film was compressed to the limits of the Langmuir trough. Monitoring π, defined as the difference in the surface tension of pure water and the surface containing the film ($\pi = \gamma_0 - \gamma$), as a function of available area A (recorded as total available trough area) resulted in the π−A isotherm. For each of five spreading solution concentrations between 0.10 and 2.0 mg/mL, five blend compositions were investigated (f = 0, 0.25, 0.50, 0.75, 1.0); three replicate depositions and compression isotherm trials were obtained for each composition and concentration.

Langmuir−Blodgett Transfer of PS-CdS/PS-*b*-PEO Films. Langmuir−Blodgett films of PS-CdS/PS-*b*-PEO blends were prepared in an analogous fashion to those described above, on the KSV 3000 LB trough equipped with a KSV dipper. For all experiments, the subphase temperature was 21 ± 0.5 °C. To optimize the transfer ratio, 0.05 mg of material (half the mass used in the isothermal studies) was deposited at the air−water interface. Several experiments confirmed that the structures were identical regardless of the mass deposited. The procedure consisted of deposition, followed a 15 min wait period for solvent evaporation, and then subsequent compression at 10 mm/min to the desired transfer pressure π. This π was maintained for 10 min before an upward vertical transfer of the Langmuir film yielded the LB films on the appropriate substrate for either AFM or TEM studies. The film transfer was completed by withdrawing the submerged substrate at a rate of 1 mm/min, yielding transfer ratios that were ∼1.0. All transferred thin films were dried vertically for a minimum of 12 h and imaged within a week.

Glass substrates used for the AFM investigations (VWR Scientific, 18 × 18 mm) were cleaned through sonication (20 min) in spectroscopic grade chloroform (99.8%, Aldrich). TEM substrates were prepared in the following manner: Cu grids (SPM Labs) were fixed onto glass by first floating a thin film of Formvar (SPM Labs) over a deionized water subphase, transferring 3−5 Cu TEM grids (SPM; 300 mesh) to the floating Formvar film, and then scooping the grid/Formvar film onto a clean glass substrate (VWR 18 × 18 mm) so that the grids were sandwiched between the Formvar and glass. After drying overnight under a dust shield, a thin layer of carbon was evaporated onto the TEM substrates.

To allow transfer of LB films to both substrate types simultaneously, a clean glass slide for AFM analysis and a glass slide with several attached TEM grids were held in tandem on a modified dipper head. Both substrates were held to the Blodgett dipper through clean binder clips affixed to a 3 in. × 1 in. microscope slide.

Atomic Force Microscopy (AFM). LB films on glass substrates were imaged on a Veeco (ThermoMicroscopes Explorer) instrument equipped with a Veeco tip (Nanoprobe-MLCT-EXMT-A) operating in contact mode. A typical image was 10 μm × 10 μm and acquired at a tip scanning rate of ∼10 μm/s. To minimize vibration-induced abnormalities in the image, the AFM probe was housed on a vibration isolation platform maintained at 80 psi and covered with a vibration dampening shield in all cases. Each sample was imaged several times at different locations on the substrate for statistical analysis of feature dimensions. The images presented were representative of a typical image at given spreading solution concentration and blend composition.

Transmission Electron Microscopy (TEM). TEM was performed on a Hitachi H-700 electron microscope, operating at an electron accelerating voltage of 75 kV. The PS-CdS/PS-*b*-PEO blend films transferred via the LB method onto the Formvar/Cu grids were used in the investigation. Qualitatively, the structures observed under the electron beam were very similar to the AFM images, suggesting that LB transfer to the disparate substrates had negligible influence on the morphologies or predominance of surface features.

Results and Discussion

UV−Vis Absorption Spectroscopy and TEM of PS-CdS. The well-known effect of quantum confinement was employed to determine the average size of QDs inside the PS-CdS building blocks, using UV−vis absorption spectroscopy of a solution of PS-CdS in chloroform. The UV−vis absorption spectrum (Figure 1a) shows an exciton shoulder and absorption edge (λ_e) at 467 nm, which was used to determine a mean CdS core

Table 2. Characteristics of the Polystyrene-*block*-poly(ethylene Oxide) Copolymers Used in This Study

PS-*b*-PEO	M_n (g/mol)	PEO (wt %)	M_w/M_n	$M_{n,PEO}$ (g/mol)	$M_{n,PS}$ (g/mol)	$x_{n,PEO}$	$x_{n,PS}$
141K	141 100	11.4	1.04	16 100	125 000	370	1200
185K	185 000	18.9	1.09	35 000	150 000	800	1440

Scheme 2. Cooperative Self-Assembly of PS-CdS and PS-*b*-PEO at the Air−Water Interface

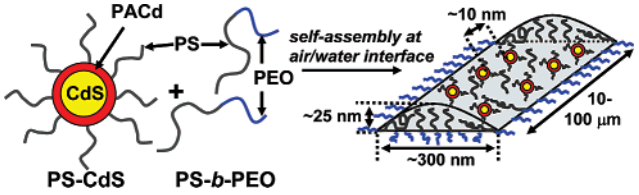

diameter ($2r_{CdS}$) of 4.1 nm through Henglein's empirical relationship.[1,32] Photoluminescence of PS-CdS dispersed in chloroform reveals a single broad red-shifted peak at ~620 nm, attributed to trap-state emission from the block copolymer-encapsulated QDs.

To directly observe the size distribution of the CdS QDs in the PS−CdS cores, we turned to transmission electron microscopy (TEM). The polymer component of PS-CdS is relatively transparent to the accelerated electrons while the CdS cores are not, therefore providing good contrast and a discernible means to measure their size. By depositing films of PS-CdS at the water surface (without added PS-*b*-PEO, corresponding to a blend composition of $f = 1$) and subsequent transfer to TEM grids, we observed polydisperse islands of PS-CdS aggregates; many of the smaller islands were determined to be monolayers of CdS nanoparticles, which allowed the QD size distributions to be conveniently assessed. By direct observation of over 250 CdS cores taken from 5 LB films, the CdS QDs were found to have a mean diameter of 3.6 nm (standard deviation of 1.3 nm), as shown in Figure 1b. The relatively broad size distribution directly observed through TEM is consistent with the lack of a sharp exciton maximum in the UV−vis spectrum. As well, the mean sizes determined by both methods are also consistent, indicating a CdS QD size of ~4 nm within each PS-CdS particle, as represented in Scheme 1. Scheme 1 also indicates the overall hydrodynamic diameter of the polymer-stabilized particles including the PS brush layer (~28 nm), as determined by dynamic light scattering (Supporting Information).

Overview of Synergistic Self-Assembly of PS-CdS/PS-*b*-PEO Blends at the Air−Water Interface. We have previously described that aggregate formation of PS-*b*-PEO copolymers at the air−water interface can be used to direct the assembly of QDs into mesoscale 1D QD/polymer surface features, including wires, cables, and rings.[22] Blends in chloroform solutions of PS-CdS with PS-*b*-PEO diblock copolymers were prepared then deposited at the air−water interface; following complete solvent evaporation, the resulting hybrid surface features were transferred to solid substrates at constant surface pressure for AFM and TEM characterization. The "PS-like" nature of PS-CdS results in athermal interactions between the QD building blocks and the PS blocks of PS-*b*-PEO (Flory−Huggins parameter $\chi = 0$), such that PS-CdS interacted preferentially with the PS component of the copolymer as the solvent evaporated and PS-*b*-PEO self-assembled, resulting in QD incorporation into various 1D (lateral aspect ratios $\gg 1$) PS surface aggregates (Scheme 2).

Figure 2 shows an interesting example of extremely long 1D self-assembled QD/polymer aggregates (which we term cables), formed from blends of PS-CdS/141K PS-*b*-PEO copolymer (Table 2) at the air−water interface. From the AFM images, these cables are found to have an average height of ~20 nm and average width of ~300 nm. A relatively low magnification AFM image of one of these very long and tortuous cables (Figure 2a) shows a single branched and interconnected QD/polymer network, which forms a number of loops and hairpin turns, and is in several regions folded multiple times on itself. The contour lengths of such branched and winding cables are difficult to accurately determine, though in certain regions it is possible to follow the length of a single aggregate up to 100 μm. Despite certain irregularities within these self-assembled structures, the widths of the cables are quite uniform along their extremely long lengths. We remark that such long and branched cables containing a uniform distribution of photoluminescent CdS QDs, with average widths on the order of optical wavelengths, represent potentially interesting photonic structures that cannot be formed via self-assembly of block copolymers in the bulk. Figure 2b,c shows higher magnification AFM images of interesting features within the branched cable network, including a typical branch point (b) and a QD/polymer ring incorporated into the cable (c). Figure 2d is a typical TEM image of a 1D aggregate from the same spreading conditions, confirming that CdS QDs are distributed uniformly throughout these long and interconnected cables.

The smooth hairpin-type folding and looping of the cable network without evidence of rupture (Figure 2a) is evidence of the mechanical stability of the QD/polymer aggregates following solvent evaporation. Along with providing a dielectric medium for the photoluminescent CdS QDs for potential photonic applications, the PS matrix imparts significant mechanical resilience, with the assemblies being kinetically "locked" by the glassy nature of PS at room temperature following evaporation of chloroform. The stability of these hybrid features contrasts previous work on QD assembly at the air−water interface where wirelike organizations of QDs were unstable on compression and expansion.[5] The various QD/polymer surface features were also found to be stable to changes in the LB surface pressure. For example, several PS-CdS/185K Langmuir films were transferred at $\pi = 2.0$, 5.0, 10, and 20 mN/m, and the observed morphologies had no discernible dependence on the transfer pressure.

Control of QD/Polymer Surface Morphologies via Blend Composition and Spreading Concentration. In studies of PS-*b*-PEO self-assembly at the air−water interface, it has been recently established that varying the concentration of the spreading solution affords control over the predominance of certain surface features.[25,26] This effect has been related to the importance of PS chain entanglements in the spreading solution, which will influence chain mobility, and therefore the extent of aggregate evolution, before kinetic trapping of morphologies by solvent evaporation. Here we describe the effect of spreading concentration on PS-CdS/PS-*b*-PEO blends as a means to tune the resultant QD/polymer structures. In addition, for a given spreading concentration, we show that the PS-CdS weight fraction f of the blends provides a further handle on morphological control. Figures 3 and 4 summarize the effects of blend composition and spreading concentration on self-assembled surface morphologies from PS-CdS/141K and PS-CdS/185K blends, respectively. For both sets of blends, two main classes of 1D aggregates were identified over the various spreading conditions: (1) wires and cables exhibiting generally uniform height and width along the length of the aggregate, or in which variations in dimensions are nonperiodic in nature, and (2) aggregates showing a periodic variation in height and width along their length, where the taller and wider regions will be referred to as "nodules" and the shorter and thinner regions between nodules will be referred to as "strands". In addition to these two classes of 1D QD/polymer aggregates, many blends also showed the existence of a large number of circular aggregates, either small dots or larger islands. Statistical analysis

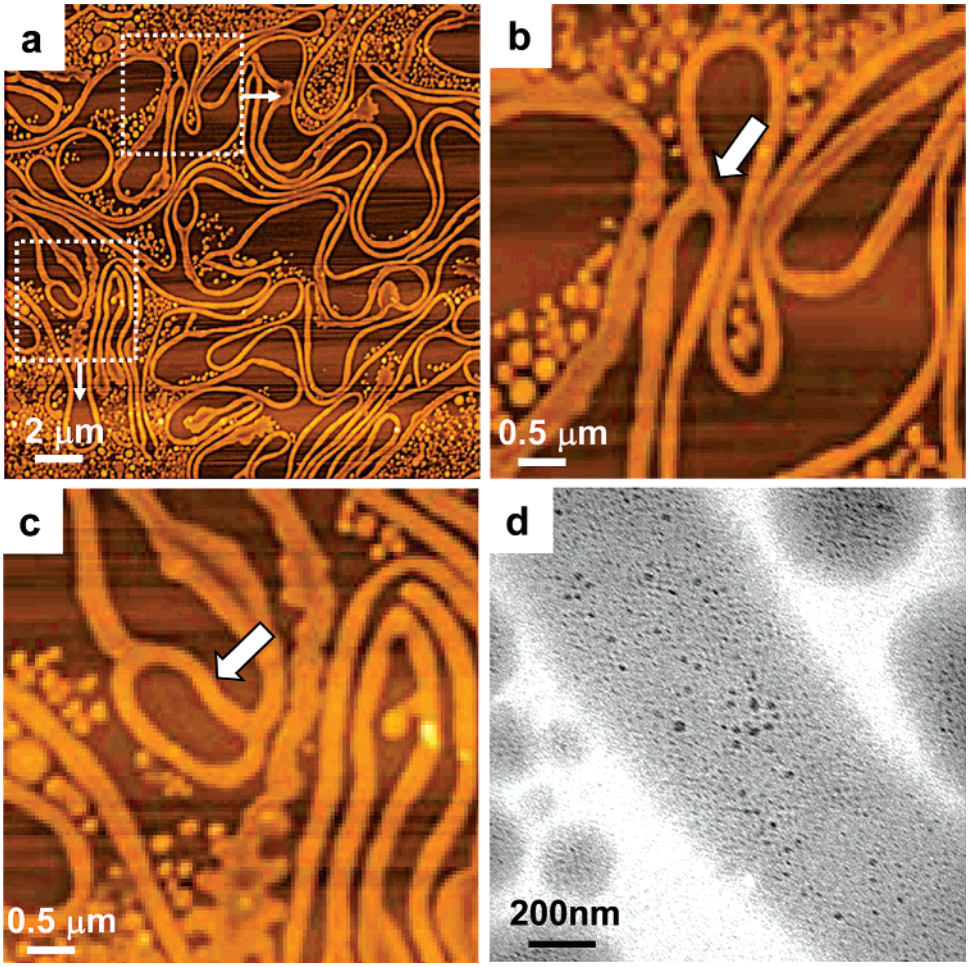

Figure 2. (a−c) AFM images of LB film from blend of PS-CdS and 141K copolymer ($f = 0.75$) deposited onto the air−water interface from 1.0 mg/mL chloroform solution. Arrows in higher magnification images in (b) and (c) indicate features described in the text. (d) TEM image of representative hierarchical assemblies from same LB film as shown in (a−c). LB film transfer occurred at 2.0 mN/m.

of the heights and widths of wires/cables, nodules, and strands from AFM data were carried out for the range of spreading conditions for the 141K and 185K blends, and mean dimensions of the various features are summarized in Tables 3 and 4, respectively.

The representative AFM images in Figures 3 and 4 show that blends containing the 141K copolymer and blends containing the 185K copolymer exhibited some similar qualitative trends with respect to changes in morphological characteristics as the blend composition and spreading concentration were varied**.** In both sets of blends, the lowest PS-CdS weight fraction ($f = 0.25$) at all spreading concentrations gave rise to 1D aggregates that were predominantly periodic, consisting of nodules and strands, with no observed wires or cables of uniform height and width. Conversely, at the highest PS-CdS weight fraction for the blends ($f = 0.75$), there was no evidence of 1D aggregates consisting of nodules and strands, and all of the 1D structures showed uniform or nonperiodic dimensions along their lengths. An additional feature of the $f = 0.75$ blends was the formation of rings incorporated into cables and wires (such as highlighted in Figure 2c), which were rarely observed at blend compositions $f < 0.75$; a few of these structures are indicated with arrows in Figures 3 and 4. The radii of these rings were generally <2 μm with wall dimensions commensurate with wires and cables. The intermediate composition ($f = 0.50$) showed morphologies with characteristics between those of the $f = 0.25$ and $f = 0.75$ blends, as some 1D aggregates with nodules and strands were noted together with wires and cables of uniform dimensions.

By varying the concentration of the spreading solutions, additional morphological control could be achieved for a given blend composition. For more concentrated spreading solutions, both periodic and nonperiodic 1D aggregates generally exhibited a higher density of branch points along their length than those formed under more dilute spreading conditions. In addition, the proportion of 1D aggregates relative to circular aggregates (dots and islands) showed a dramatic dependence on spreading concentration. For both sets of blends (141K and 185K copolymers) and for all three blend compositions, a spreading concentration of 2.0 mg/mL yielded predominantly 1D aggregates, whereas more dilute spreading conditions resulted in an increase in the proportion of islands and dots. In fact, the lowest spreading concentration for all blends containing the 185K copolymer yielded too few 1D aggregates to carry out statistical analysis of feature dimensions (Table 4). Along with demonstrating control over self-assembled QD/polymer aggregates, the concentration and composition dependence of aggregate morphology summarized in Figures 3 and 4 provides important clues into the formation and evolution of these structures; these mechanistic aspects will be discussed in a future section.

Whereas TEM images show CdS QDs to be uniformly distributed throughout nonperiodic wires and cables (Figure 2d), 1D aggregates possessing periodic variations in dimensions

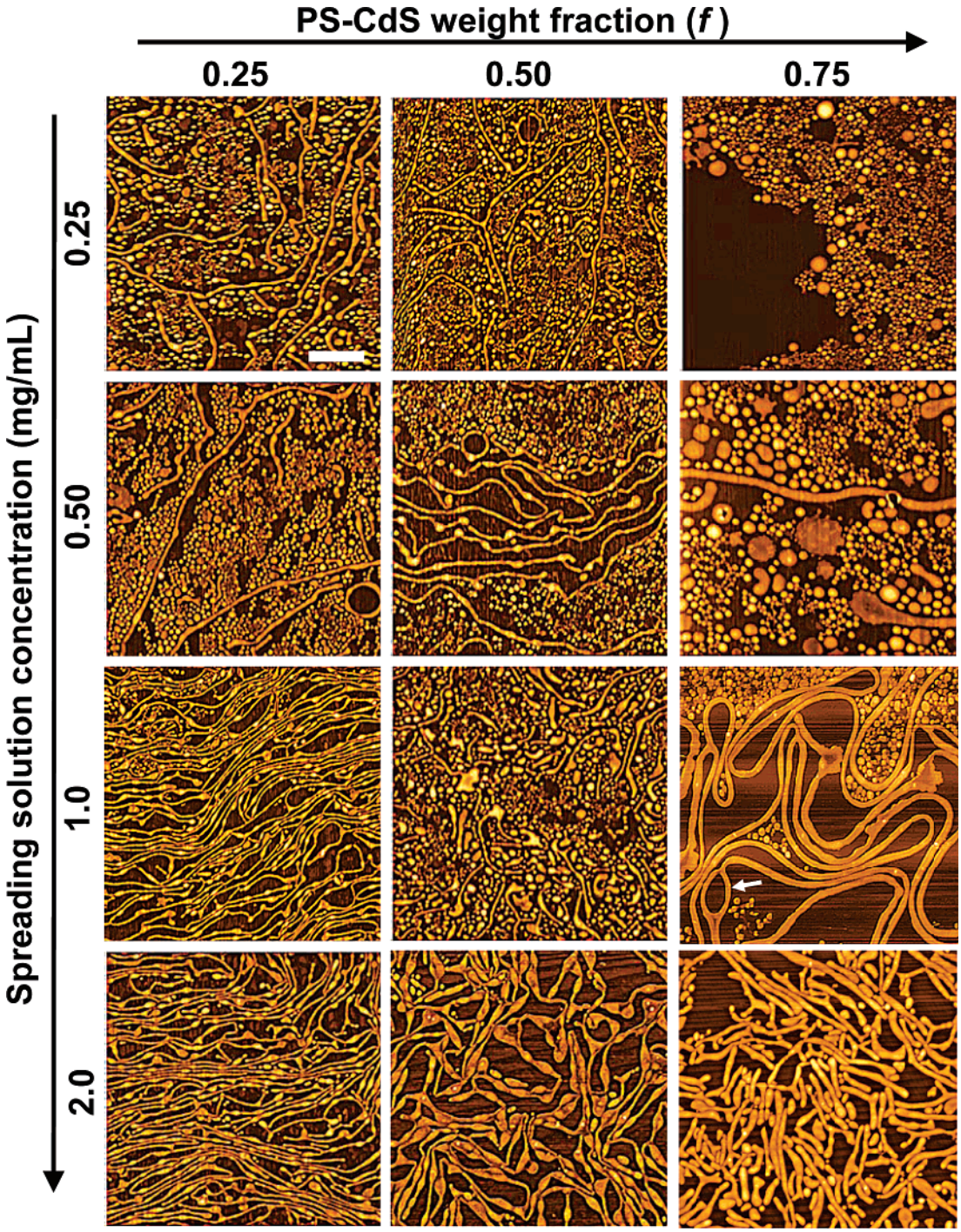

Figure 3. Representative AFM images of PS−CdS/141K LB films self-assembled under various spreading conditions and transferred at 2.0 mN/m. Scale bar represents 2 μm and is consistent for all images.

along their length reveal an internal structure in which the CdS QDs are located only within the nodules (Figure 5); this suggests that nodules are regions in which PS-CdS are localized within spaghetti aggregates formed by the PS-*b*-PEO component. This conclusion is also supported by the mean heights and widths of strands within periodic 1D aggregates for both sets of blends (Tables 3 and 4), which are consistent under different spreading conditions and nearly identical to the mean dimensions of spaghetti aggregates formed from the respective PS-*b*-PEO copolymer component on its own ($h = 12$ nm and $w = 160$ nm for 141K and $h = 15$ nm and $w = 170$ nm for 185K). On the other hand, the mean widths of nodules in both sets of blends are about 2 times the widths of the strands between them, on the order of 300 nm, showing some variability for different spreading conditions; the nodules, containing localized PS-CdS, are therefore approximately the same width as the wires and cables which contain PS-CdS distributed uniformly throughout the aggregate. The heights of the nodules are also nearly identical to the heights of wires and cables for blends containing a given copolymer: $h \sim 20$ nm for blends containing 141K and $h \sim 27$ nm for blends containing the 185K copolymer. The taller wires, cables, and nodules for the 185K blends compared to the 141K blends, independent of composition and spreading concentration, are consistent with a taller brush formed from the longer PS blocks and further support that PS-CdS particles are intercalated as a monolayer into the PS-*b*-PEO brush structure.

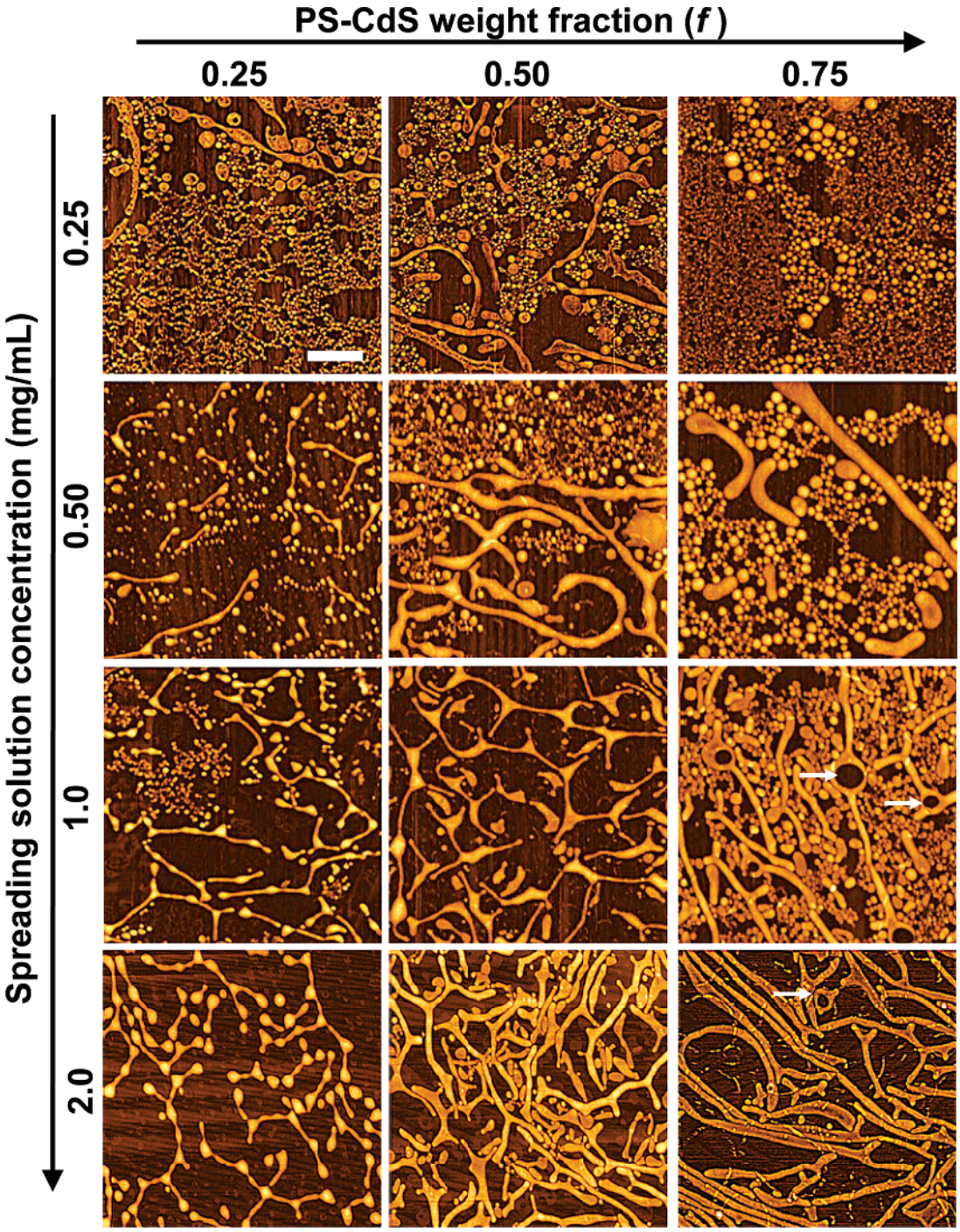

Figure 4. Representative AFM images of PS-CdS/185K LB films self-assembled under various spreading conditions and transferred at 5.0 mN/m. Scale bar represents 2 μm and is consistent for all images.

Finally, we point out that statistical analysis of mean feature dimensions reveals the general trend that the average width of QD/polymer wires and cables tends to increase with decreasing spreading concentration; this is most clearly shown for the series of PS-CdS/185K blends with composition $f = 0.75$, where the mean aggregate width increases from 320 to 560 nm as the spreading concentration decreases from 2.0 to 0.50 mg/mL (Table 4). Such tunability of the widths of QD/polymer composite wires via self-assembly, independent of the size and emission wavelength of the constituent QDs, is very promising for their future application as active waveguides in photonic circuits, since the emission wavelength and waveguide dimensions would have to be properly matched to allow for single-mode propagation of light through the wires.[34]

Surface Pressure−Area Isotherms of QD/Polymer Features at the Air−Water Interface. Previous investigations of interfacial self-assembly of PS-*b*-PEO have shown that $\pi-A$ isotherms of surface aggregates following evaporation of the spreading solvent reveal pertinent information on aggregate structure at the air−water interface, complementing AFM data from transferred LB films.[25−28] AFM and TEM provide structural information on the glassy PS cores of the surface aggregates alone, whereas compression isotherms give insight into the dimensions and conformation of the PEO chains within aggregates at the water surface. Analysis of isotherm data from pure PS-*b*-PEO films has led to the generally accepted conclusion that for aggregates at low surface density PEO blocks radiate out from various PS core structures as a 2D corona at

Table 3. Mean Dimensions of Surface Aggregates from Self-Assembly of PS-CdS/141K PS-*b*-PEO Blends at the Air−Water Interface[a]

		wires/cables		nodules		strands	
spread concn (mg/mL)	*f*	*h* (nm)	*w* (nm)	*h* (nm)	*w* (nm)	*h* (nm)	*w* (nm)
	0.25			19 ± 3	280 ± 50	11 ± 2	170 ± 30
0.25	0.50			19 ± 4	290 ± 40	11 ± 1	150 ± 30
	0.75						
	0.25			19 ± 4	320 ± 40	11 ± 2	170 ± 30
0.50	0.50			20 ± 3	340 ± 40	11 ± 1	180 ± 30
	0.75	20 ± 2	420 ± 50				
	0.25			18 ± 2	240 ± 50	12 ± 2	140 ± 20
1.0	0.50	20 ± 2	300 ± 40	19 ± 3	290 ± 50	10 ± 2	160 ± 20
	0.75	21 ± 2	280 ± 50				
	0.25			20 ± 3	260 ± 60	12 ± 1	150 ± 20
2.0	0.50	19 ± 4	320 ± 60				
	0.75	21 ± 2	320 ± 40				

[a] Error represents the standard deviation determined from at least 25 surface features.

Table 4. Mean Dimensions of Surface Aggregates from Self-Assembly of PS-CdS/185K PS-*b*-PEO Blends at the Air−Water Interface[a,b]

		wires/cables		nodules		strands	
spread concn (mg/mL)	*f*	*h* (nm)	*w* (nm)	*h* (nm)	*w* (nm)	*h* (nm)	*w* (nm)
	0.25			27 ± 3	360 ± 40	15 ± 2	180 ± 30
0.50	0.50	24 ± 3	430 ± 80				
	0.75	28 ± 3	560 ± 90				
	0.25			26 ± 2	320 ± 40	16 ± 2	170 ± 20
1.0	0.50	28 ± 5	380 ± 110				
	0.75	29 ± 5	370 ± 80				
	0.25			26 ± 4	310 ± 60	15 ± 2	180 ± 30
2.0	0.50	24 ± 5	310 ± 40				
	0.75	27 ± 3	320 ± 30				

[a] Error represents the standard deviation determined from at least 25 surface features. [b] 0.25 mg/mL spreading concentration showed mainly polydisperse islands at all compositions, with very few 1D aggregates.

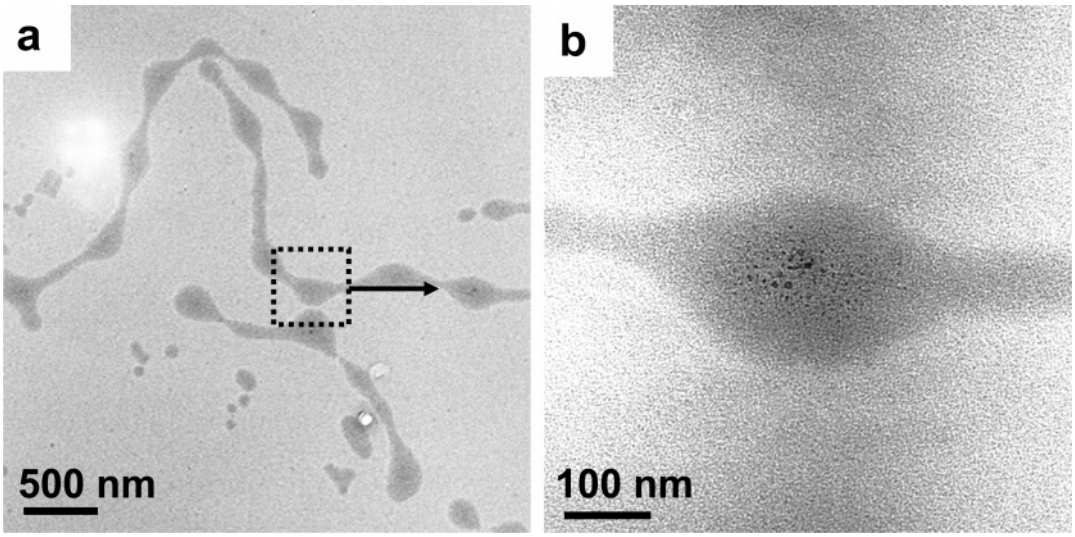

Figure 5. TEM images of PS-CdS/185K blend ($f = 0.25$, spreading concentration = 2.0 mg/mL), showing periodic 1D structures. Higher magnification image in (b) shows CdS QDs localized in wider nodules.

the water surface ("pancake" conformation).[25−28] A recent model from Cox et al. suggests that some PEO chains are also trapped underneath the PS cores.[35] When aggregates on the water surface are laterally compressed, their surface density increases until PEO chains in neighboring corona eventually overlap, resulting in an increase in the surface pressure (π) until coronal PEO chains submerge into the subphase to form a PEO brush; this conformational change upon compression is commonly described as the "pancake-to-brush" phase transition and is observed as a pseudoplateau in the $\pi-A$ isotherm at constant $\pi \sim 10$ mN/m. Further compression results in contact between the relatively incompressible PS cores and a sharp increase in π. The extent of the pseudoplateau has been found to be dependent on the PEO content: for copolymers with less than ~15 wt % PEO, the PEO pancake-to-brush transition is generally impeded by the large relative surface area of the PS cores, such that a pseudoplateau is not observed.[25,26]

Compression isotherms were first obtained for the pure 141K or 185K copolymers ($f = 0$, Figures 6a and 7a, respectively). Both of these show an initial gradual increase in π as A is decreased (pancake regime), indicating the overlap of PEO coronal chains, although only the more hydrophilic 185K copolymer exhibits a detectable pseudoplateau. The subsequent relatively sharp increase in π at lower A for both copolymers (brush regime) indicates steric repulsion of PS cores. In contrast, the compression isotherm of pure PS−CdS ($f = 1$, Figures 6a

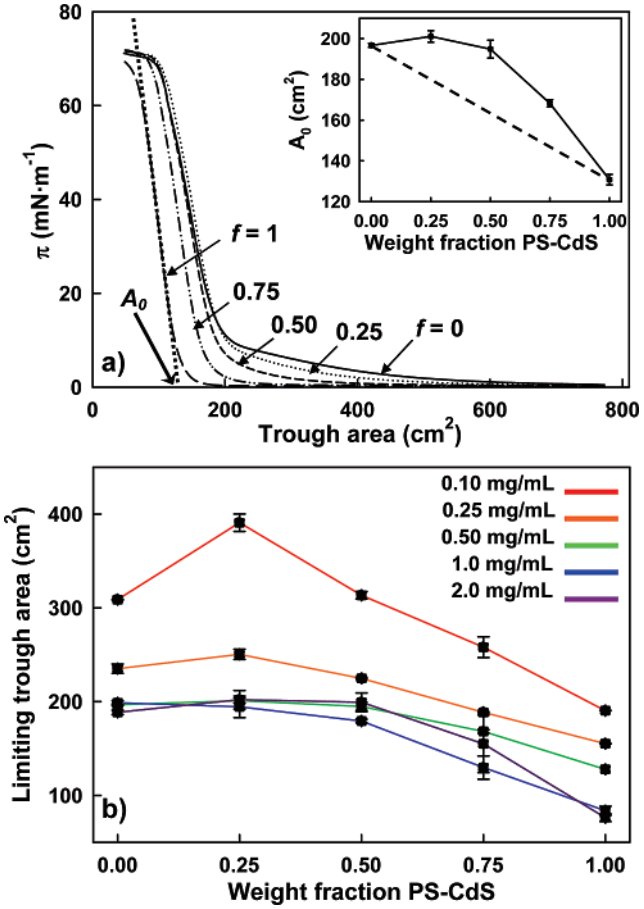

Figure 6. (a) Langmuir isotherms of PS-CdS/141K blends at the air−water interface from spreading concentrations of 0.50 mg/mL and variable PS-CdS weight fraction (f), showing determination of limiting area (A_0) for $f = 1.0$ for example. Inset shows plot of A_0 vs f for the isotherms in (a) along with the hypothetical linear plot. (b) Plots of A_0 vs f for various spreading concentrations indicated in the figure.

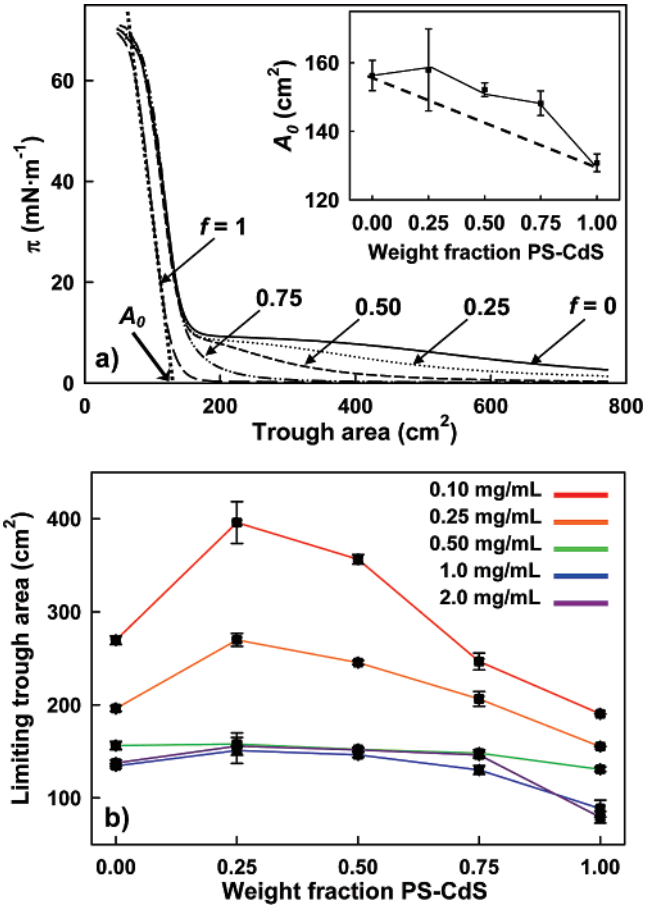

Figure 7. (a) Langmuir isotherms of PS-CdS/185K blends at the air−water interface from spreading concentrations of 0.50 mg/mL and variable PS-CdS weight fraction (f), showing determination of limiting area (A_0) for $f = 1.0$ for example. Inset shows plot of A_0 vs f for the isotherms in (a) along with the hypothetical linear plot. (b) Plots of A_0 vs f for various spreading concentrations indicated in the figure.

and 7a) shows no initial gradual increase in π, with only a single sharp rise in surface pressure at a trough area that is low compared to the onset of the brush regime for both copolymers. The $f = 1$ isotherm is thus consistent with what has been previously observed for monolayers of pure PS homopolymer; this is explained by the PS-like nature of PS-CdS, which forms low-compressibility aggregates at the water surface that repel one another upon film compression without the initial soft interactions of intervening PEO chains. For blends of both components at the air−water interface, the gradual addition of PS-CdS caused the isotherms to change markedly from those of the pure copolymers, increasingly resembling pure PS-CdS (Figures 6a and 7a). For the PS-CdS/185K blends, where a pseudoplateau was evident in the compression isotherm of the pure copolymer, the increasing incorporation of PS-CdS into the surface aggregates resulted in the PEO phase transition becoming increasingly hindered, decreasing the extent of the pseudoplateau (Figure 7a). The limiting area A_0 for each blend composition and spreading concentration was determined from extrapolation of the steepest part of the isotherm to $\pi = 0$, as shown in Figures 6a and 7a. If the limiting area of each component was independent of the amount of the other component, a linear relationship between A_0 and the blend composition would be expected, as represented by the dashed line in the insets of Figures 6a and 7a. However, actual plots of A_0 vs f are clearly nonlinear for every spreading concentration (Figures 6b and 7b), with A_0 values for the blends lying consistently above the hypothetical linear plot. Along with the AFM and TEM data discussed previously, this nonlinearity suggests that the self-assembly of PS-CdS/PS-*b*-PEO blends is synergistic in nature, with the presence of one component influencing the surface conformation of the other. However, we have shown in previous work that the surface conformation of pure PS-*b*-PEO is also affected by its spreading concentration due to chain entanglement effects;[25] this effect is evident in the increasing A_0 values at $f = 0$ with decreasing spreading concentration (Figures 6b and 7b). Since the spreading concentration of PS-*b*-PEO copolymers within blend solutions will decrease with increasing f for a constant overall spreading concentration, independent of possible interactions with PS-CdS, interpretation of the isotherms is complicated by a number of possible factors.

For all blends and at all spreading concentrations, plots of A_0 vs f exhibit a clear maximum (Figures 6b and 7b), with an initial increase in limiting area when PS-CdS is added to $f = 0.25$, followed by a nonlinear decrease as the PS-CdS content is further increased. The initial increases in A_0 are found to be more dramatic, and the overall A_0 values are found to be higher, when blend solutions are cast in the dilute regime (i.e., $\leq$ 0.25 mg/mL). We attribute the observed maxima in A_0 to two competing effects of increasing the PS-CdS content in the blend solutions. First, there is a "dilution effect", where an increase in the PS-CdS content at constant overall concentration will result in dilution of the copolymer in the spreading solution, resulting in an increase in the limiting area of PS-*b*-PEO at the water surface due to a decrease in entanglements of the long

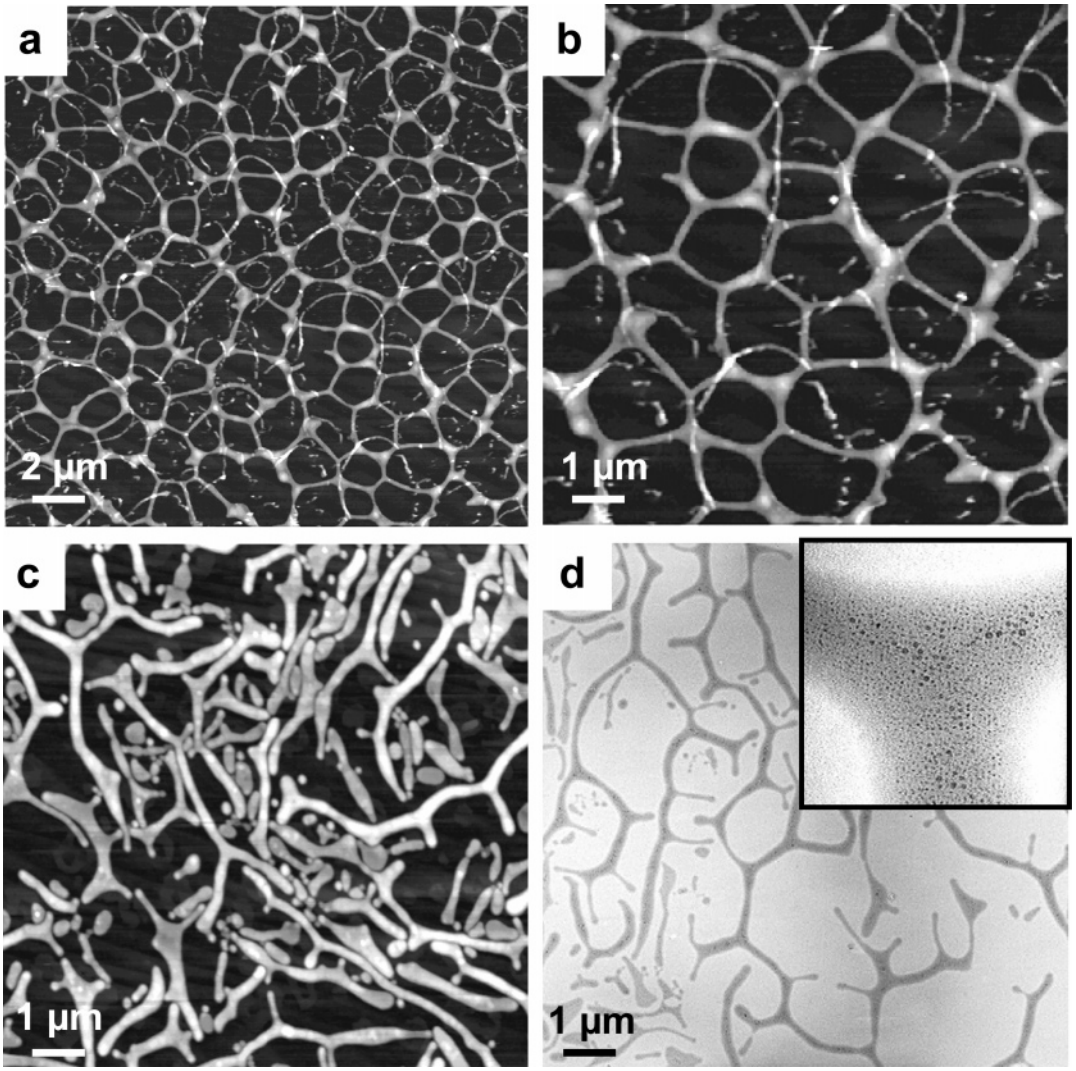

Figure 8. AFM (a−c) and TEM (d) images of LB film from blend of PS-CdS and 185K copolymer ($f = 0.50$) deposited onto the air−water interface from 2.0 mg/mL chloroform solution. Polygonal network pattern (a, b) coexists on same LB film with branched wire aggregates (c, d), suggesting wires and cables form via breaks in connectivity within a network pattern arising from solution dewetting. TEM image shows uniform distribution of CdS QDs within branched wires; edge length of inset is 500 nm. LB film transfer occurred at 5.0 mN/m.

PS blocks. Second, an increase in PS-CdS content will tend to make the interfacial behavior of the blends more like pure PS-CdS, affecting a decrease in the limiting area. The competition between these two effects results in the observed maxima at $f = 0.25$ as the PS-CdS content increases. In addition, the role of PS-*b*-PEO dilution explains why the initial increase in A_0 is more prominent at lower spreading concentrations, since chain entanglements are more significantly affected by dilution below a critical concentration of the copolymer.

Mechanism of Synergistic Self-Assembly: Role of Dewetting. The dependence of spreading concentration on the observed morphologies of self-assembled QD/polymer surface features points to the important kinetic effect of polymer entanglements in the spreading solution. Similar to the spreading concentration dependence of pure PS-*b*-PEO diblock copolymers at the air−water interface reported previously,[25,26,39] the various 1D QD/polymer structures observed in this work are seen to represent a range of kinetically trapped states, where structure evolution and ultimate freezing of the aggregates are both the result of solvent evaporation. Since higher spreading concentrations result in slower chain dynamics in the spreading solution before freezing occurs, they give rise to earlier snapshots in the process of structure formation and evolution.[25] On the basis of these arguments, we look to certain aggregate morphologies from blends at the highest spreading concentration (2.0 mg/mL), which suggest that dewetting of the evaporating blend solution from the water surface plays a key role in the initial stages of self-assembly.

The conditions and mechanism for dewetting of liquid polymer films from solid and liquid surfaces are well-known.[36−38] Under conditions where long-range van der Waals interactions predominate, the tendency of a thin film ($\ll 1\ \mu$m) to undergo dewetting is determined by the sign of the effective Hamaker constant, $A = A_{LL} - A_{SL}$, where A_{LL} is the Hamaker constant for liquid−liquid interactions within the film and A_{SL} is the Hamaker constant for substrate−liquid interactions. If A is positive, then cohesive interactions within the film are stronger than interactions between the film and the substrate, and the film will dewet in order to minimize contact with the substrate.[37] Film rupture results in the formation of holes throughout the film, which expand as material flows from wet regions into raised rims surrounding the growing holes. Advancing rims eventually come into contact, forming a polygon pattern of interconnected liquid ribbons which finally breaks down into droplets via a Rayleigh instability.[36,38]

LB films of a PS-CdS/185K blend (PS-CdS content $f = 0.5$) from a spreading concentration of 2.0 mg/mL showed regions consisting of a highly interconnected polygonal network (Figure

8a,b), strongly reminiscent of patterns formed in the intermediate stages of dewetting of thin polystyrene films from solid surfaces,[36,38] with an apparent bias toward hexagonal holes and most vertices connecting three edges within the network.[36] These networks were found to coexist with highly branched QD/polymer wires within the same LB films (Figure 8c,d). In particular, the TEM image in Figure 8d shows branched QD/polymer wires interconnected in a manner which suggests a "broken" network of polygonal holes, providing a mechanistic link between the networks and the evolution of 1D wires. This combination of features suggests a mechanism of self-assembly initiated by dewetting of a continuous film of PS-CdS/PS-*b*-PEO in chloroform from the water surface due to increasing contributions from unfavorable PS−water interactions as the spreading solvent evaporates. The solvent-swollen walls of the resulting polygonal network contain a mixture of PS-CdS and PS-*b*-PEO, with the copolymer component forming a brush structure with PEO blocks oriented toward the water surface and PS block oriented toward the chloroform at the interface. The networks then appear to evolve via breaks in connectivity (Figure 8c,d) to form the various observed branched and 1D polymer features containing QDs. We have recently described similar dewetting patterns and transitional structures leading to 1D aggregates from the 141K PS-*b*-PEO copolymer on its own at a high spreading concentration (2.0 mg/mL);[39] this indicates that a dewetting mechanism for aggregate formation is not unique to the blend systems, with the main difference of the blends being that the dewetting PS-*b*-PEO brush is mixed with the PS-CdS particles which are intercolated throughout the solvent-swollen PS regions.

When the concentration of PS-CdS in the QD/polymer features is relatively low (e.g., $f = 0.25$, Figures 3 and 4), it appears that further solvent evaporation induces phase separation between the PS-CdS and the PS regions of the PS-*b*-PEO brush structure, resulting in the formation of nodules where the PS-CdS becomes localized; this phase separation is an entropy-driven process, similar to the autophobic phase separation of colloidal polymer brushes from a chemically identical homopolymer,[40] and is attributed to a loss in conformational entropy with interpenetration of the PS-CdS and PS-*b*-PEO brushes. It is probable that the same driving force for phase separation between PS-CdS and PS-*b*-PEO exists at higher PS-CdS content (e.g., $f = 0.75$), except that the high concentration of PS-CdS in the solvent-swollen composite features results in restricted lateral mobility of the QDs. For this reason, nodule formation cannot occur before the structures are locked in by vitrification, resulting in the various described 1D composite features containing a uniform distribution of CdS QDs.

Finally, AFM data also suggest that solution dewetting from the water surface can also account for the formation of novel QD/polymer rings incorporated into cables, which is a predominant surface feature for blends at relatively high PS-CdS content ($f = 0.75$, Figures 3 and 4). It was noted that several of the LB films containing ring/cable structures also contained small planar aggregates along the length of the cables where an elevated rim was present at the edge of a relatively flat surface, similar to a continent as described by Devereaux et al.[26] It appears that these flat surfaces tend to rupture by formation of a single central hole in a secondary dewetting process, followed by the radial growth of the hole. Figure 9 provides a pictorial representation of this secondary dewetting process resulting in rings of various radii and at various stages of their development. The series of structures (i−iii) indicated in Figure 9 provides evidence for this morphological evolution

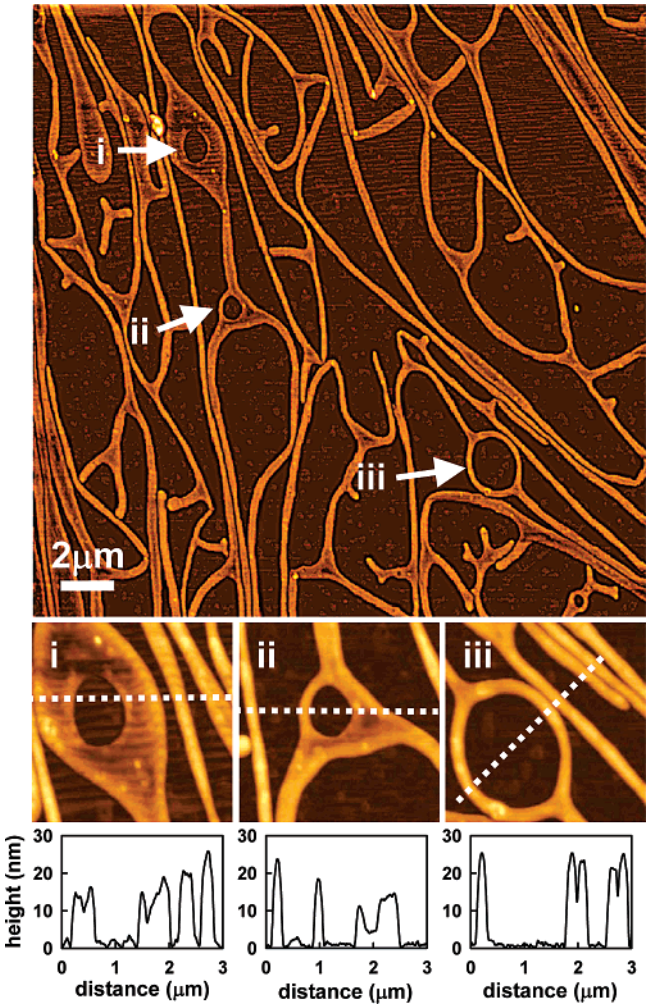

Figure 9. AFM image of a LB film from blend of PS-CdS and 185K copolymer ($f = 0.75$) deposited onto the air−water interface from 2.0 mg/mL chloroform solution and transferred at 5.0 mN/m. Magnified images of indicated regions highlight various kinetic snapshots in the formation and evolution of rings; arrows indicate the respective magnified images and height profiles (i−iii).

where (i) is vitrified at the stage of initial hole formation in a continent structure, a process which leads to the eventual development of a mature ring (iii). The accompanying topology profiles show that the height of the rim formed around the hole after the initial rupture (i, ∼15 nm) is significantly less than the height of a mature ring (iii, ∼25 nm); this further suggests a dewetting process where hole growth pushes copolymer material into to the rim as it matures, resulting in increased brush density and height.

Conclusions

This work details several important aspects of organizing polymer-stabilized CdS QDs into mesoscale hierarchical structures via synergistic self-assembly with PS-*b*-PEO diblock copolymers at the air−water interface. By this spontaneous process, QDs with a surrounding PS brush layer (PS-CdS) can be incorporated into various 1D QD/polymer structures with widths commensurate with optical wavelengths ∼300 nm, including wires and cables containing a uniform distribution of semiconductor QDs. Under different spreading conditions, periodic 1D aggregates were also formed with QD-containing nodules alternating along the long axes with thinner strands that do not contain QDs. Additionally, pseudo-1D hybrid structures were formed including branched wires and rings incorporated

along the lengths of cables. Some control over morphology was achieved by varying the PS-CdS/PS-*b*-PEO blend composition and the concentration of the spreading solution. Higher PS-CdS fractions resulted in more uniform distribution of QDs throughout 1D QD/polymer structures, whereas lower PS-CdS fractions gave rise to periodic structures containing of nodules of localized QDs. For higher spreading concentrations, 1D aggregates were found to be more predominant and more highly branched, compared to lower spreading concentrations, which resulted in less-branched 1D structures and an increased predominance of circular aggregates. It is important to note that, although the various observed surface features are kinetic, rather than thermodynamic structures, the general trends described in Figures 3 and 4 and Tables 3 and 4 were reproducible for separate films prepared under identical sets of conditions. This indicates some promise for using kinetic control via this method to obtain a desired mixture of hierarchical structures. Furthermore, subsequent selection and alignment of specific features may be possible via controlled LB transfer onto patterned surfaces with well-defined hydrophobic/hydrophilic regions.

A detailed investigation of $\pi-A$ isotherms of PS-CdS/PS-*b*-PEO blends at the air−water interface revealed that the interfacial behavior of the aggregates was also strongly influenced by the spreading conditions and blend composition. For all spreading concentrations, a maximum was found in plots of the limiting area vs PS-CdS weight fraction in the blends, which was explained by a competition between the conformational effects of PS-*b*-PEO dilution and PS-CdS addition. Finally, AFM data of structures obtained at the highest spreading concentration provide insight into a mechanism of formation for these QD/polymer assemblies, beginning with dewetting of the evaporating polymer solution from the air−water interface. These insights into the control of structure and interfacial behavior of 1D QD/polymer assemblies, and into their mechanism of formation, are important steps toward potential applications of this new method of hierarchical nanoparticle organization at the mesoscale.

Acknowledgment. The authors gratefully acknowledge the National Science and Engineering Research Council (NSERC), the Canadian Foundation for Innovation (CFI), and the British Columbia Knowledge Development Fund (BCKDF) for their generous support of the research. We also acknowledge Mr. Yunyong Guo for his kind assistance with the photoluminescence measurement.

Supporting Information Available: Experimental details on the preparation of PS-CdS block copolymer-stabilized CdS quantum dots; details on dynamic light scattering (DLS) measurements of PS-CdS in chloroform, including cumulant and CONTIN analysis of DLS data to determine mean particle size and size distribution information. This material is available free of charge via the Internet at http://pubs.acs.org.

References and Notes

(1) Henglein, A. *Chem. Rev.* **1989**, *89*, 1861.
(2) Tang, Z.; Kotov, N. A. *Adv. Mater.* **2005**, *17*, 951.
(3) Ujihara, M.; Mitamura, K.; Torikai, N.; Imae, T. *Langmuir* **2006**, *22*, 3656.
(4) Korth, B. D.; Keng, P.; Shim, I.; Bowles, S. E.; Tang, C.; Kowalewski, T.; Nebesny, K. W.; Pyun, J. *J. Am. Chem. Soc.* **2006**, *128*, 6562.
(5) Sear, R. P.; Chung, S.-W.; Markovich, G.; Gelbart, W. M.; Heath, J. R. *Phys. Rev. E* **1999**, *59*, 6255.
(6) Hassenkam, T.; Nørgaard, K.; Iversen, L.; Kiely, C. J.; Brust, M.; Bjørnholm, T. *Adv. Mater.* **2002**, *14*, 1126.
(7) Reuter, T.; Vidoni, O.; Torma, V.; Schmid, G.; Nan, L.; Gleiche, M.; Chi, L.; Fuchs, H. *Nano Lett.* **2002**, *2*, 709.
(8) Fahmi, A. W.; Oertel, U.; Steinert, V.; Froeck, C.; Stamm, M. *Macromol. Rapid Commun.* **2003**, *24*, 625.
(9) Rabani, E.; Reichman, D. R.; Geissler, P. L.; Brus, L. E. *Nature (London)* **2003**, *426*, 271.
(10) Maillard, M.; Motte, L.; Ngo, A. T.; Pileni, M. P. *J. Phys. Chem. B* **2000**, *104*, 11871.
(11) Shah, P. S.; Sigman, M. B.; Stowell, C. A.; Lim, K. T.; Johnston, K. P.; Korgel, B. A. *Adv. Mater.* **2003**, *15*, 971.
(12) Zhang, L.; Gaponik, N.; Müller, J.; Plate, U.; Weller, H.; Erker, G.; Fuchs, H.; Rogach, A. L.; Chi, L. *Small* **2005**, *1*, 524.
(13) Böker, A.; Lin, Y.; Chiapperini, K.; Horowitz, R.; Thompson, M.; Carreon, V.; Xu, T.; Abetz, C.; Skaff, H.; Dinsmore, A. D.; Emrick, T.; Russell, T. P. *Nat. Mater.* **2004**, *3*, 302.
(14) Haryono, A.; Binder, W. H. *Small* **2006**, *2*, 600.
(15) Lin, Y.; Böker, A.; He, J.; Sill, K.; Xiang, H.; Abetz, C.; Li, X.; Wang, J.; Emrick, T.; Long, S.; Wang, Q.; Balazs, A.; Russell, T. P. *Nature (London)* **2005**, *434*, 55.
(16) Chiu, J. J.; Kim, B. J.; Kramer, E. J.; Pine, D. J. *J. Am. Chem. Soc.* **2005**, *127*, 5036.
(17) Bockstaller, M. R.; Lapetnikov, Y.; Margel, S.; Thomas, E. L. *J. Am. Chem. Soc.* **2003**, *125*, 5276.
(18) Lopes, W. A.; Jaeger, H. M. *Nature (London)* **2001**, *414*, 735.
(19) Grohn, F.; Gu, X.; Grull, H.; Meredith, J. C.; Nisato, G.; Bauer, B. J.; Karim, A.; Amis, E. J. *Macromolecules* **2002**, *35*, 4852.
(20) Minelli, C.; Geissbuehler, I.; Eckert, R.; Vogel, H.; Heinzelmann, H.; Liley, M. *Colloid Polym. Sci.* **2004**, *282*, 1274.
(21) Wang, C.-W.; Moffitt, M. *Chem. Mater.* **2005**, *17*, 3871.
(22) Cheyne, R. B.; Moffitt, M. G. *Langmuir* **2005**, *21*, 10297.
(23) Zhu, J.; Eisenberg, A.; Lennox, R. B. *J. Am. Chem. Soc.* **1991**, *113*, 5583.
(24) Cox, J.; Eisenberg, A.; Lennox, R. B. *Curr. Opin. Colloid Interface Sci.* **1999**, *4*, 52.
(25) Cheyne, R. B.; Moffitt, M. G. *Langmuir* **2005**, *21*, 5453.
(26) Devereaux, C. A.; Baker, S. M. *Macromolecules* **2002**, *35*, 1921.
(27) Cox, J. K.; Yu, K.; Constantine, B.; Eisenberg, A.; Lennox, R. B. *Langmuir* **1999**, *15*, 7714.
(28) Kim, Y. P.; J.; Frechet, J. M. J.; Hawker, C. J.; Frank, C. W. *Langmuir* **2005**, *21*, 10444.
(29) Barrelet, C. J.; Greytak, A. B.; Lieber, C. M. *Nano Lett.* **2004**, *4*, 1981.
(30) Desjardins, A.; Eisenberg, A. *Macromolecules* **1991**, *24*, 5779.
(31) Zhong, X. F.; Varshney, S. K.; Eisenberg, A. *Macromolecules* **1992**, *25*, 7160.
(32) Moffitt, M.; McMahon, L.; Pessel, V.; Eisenberg, A. *Chem. Mater.* **1995**, *7*, 1185.
(33) Wang, C.-W.; Moffitt, M. G. *Langmuir* **2004**, *20*, 11784.
(34) Takazawa, K.; Kitahama, Y.; Kimura, Y.; Kido, G. *Nano Lett.* **2005**, *5*, 1293.
(35) Cox, J. K.; Yu, K.; Eisenberg, A.; Lennox, R. B. *Phys. Chem. Chem. Phys.* **1999**, *1*, 4417.
(36) Reiter, G. *Phys. Rev. Lett.* **1992**, *68*, 75.
(37) Bollinne, C.; Cuenot, S.; Nysten, B.; Jonas, A. M. *Eur. Phys. J. E* **2003**, *12*, 389.
(38) Muller-Buschbaum, P. *J. Phys.: Condens. Matter* **2003**, *15*, R1549.
(39) Cheyne, R. B.; Moffitt, M. G. *Langmuir* **2006**, *22*, 8387.
(40) Hasegawa, R.; Aoki, Y.; Doi, M. *Macromolecules* **1996**, *29*, 6656.

MA062355U